**Proceedings of ASME 2021**
**Fluids Engineering Division Summer Meeting**
**FEDSM2021**
**August 10-12, 2021, Virtual Conference, USA**

# FEDSM2021-65809

# AN INVESTIGATION OF THE EFFECTS OF VOLUME FRACTION ON DRAG COEFFICIENT OF NON-SPHERICAL PARTICLES USING PR-DNS

**Pratik Mahyawansi**
Department of Mechanical and Materials Engineering
Florida International University
Miami, Florida 33174
Email: pmahy002@fiu.edu

**Cheng-Xian Lin***
Department of Mechanical and Materials Engineering
Florida International University
Miami, Florida 33174
Email: lincx@fiu.edu

## ABSTRACT

*Prediction of the drag coefficient is required in gas-particle multiphase flow modeling and simulation. Experimental data and correlations on the fixed-bed system of spherical particles with high volume fractions for various possible arrangements are available in the literature. However, the effect of volume fraction on the drag coefficient of non-spherical particles is not well studied. In solving the momentum equation, the volume fraction plays a vital role in determining the flow resistances. In this paper, we study the impact of volume fraction in the range of 0.069 to 0.65 on the drag coefficient using the computational fluid dynamics (CFD) simulation of air for Reynold number in the range of 10 to 10000 using particle resolved direct numerical solution (PR-DNS). Regular non-spherical particles such as a cube, tetrahedron, and spheroids are used in this study since their single particle's drag coefficient data are available in the literature for comparison. For this work, the simulations are carried out in the Ansys Fluent using polyhedral mesh, which consumes significantly less computational time and power. The study showed the sphericity and volume fraction have significant impact on the bed pressure drop and average drag coefficient of the particles in the bed especially in high Reynolds number regime. The bed of the spheroid experiences the lowest drag being the most streamlined particle, and the particles with the edges result in a large drag coefficient due to flow separation at the discontinuity. The vector plots verify this behavior where large wake regions are observed behind the tetrahedron particle.*

## NOMENCLATURE

- $\phi$ Volume fraction
- $\psi$ Sphericity
- P Pressure ($Pa$)
- $\rho$ Density of fluid ($kg/m^3$)
- $\mu$ Dynamic viscosity ($Pa$-$s$)
- L Length of the bed ($m$)
- V Superficial velocity ($m/s$)
- $D_P$ Diameter of particle ($m$)
- $C_d$ Drag coefficient
- $A_p$ Projected area perpendicular to the flow($m^2$)
- CFL Courant–Friedrichs–Lewy
- Re Reynolds number

## INTRODUCTION

The fixed bed system finds many applications such as in chemical reactions, heat and mass transfer [1], pollutant absorption in water filtering plant [2,3], and variety of other applications where a fluid is required to pass through the bed with a constant linear velocity. The system is a packing of solid particles in an internal flow passage forming a porous medium, where the fluid passes through a complex flow path and experiences considerable flow resistance depending on the porosity or volume fraction of the bed. The packing can be either a regular lattice structure like body-centered cubic (BCC) or simple cubic (SC) or a randomly packed system. For specific applications, higher convection rates are required, for which instead of fixed-bed, the

*Corresponding author

particles can move freely with vertically upward flow under gravity's influence. They are aloft, and the bed overall might attain equilibrium with hydrodynamic and gravity forces; however, the individual particle's dynamics remain chaotic; this is called a fluidized bed. Designing such systems to meet various large scale industrial requirements cannot be accomplished using lab-scale experiments which demands numerical modeling such as porous media approach for fixed bed and discrete element model (DEM) or two-fluid model for the fluidized bed [4, 5]. These numerical models relay on drag model and pressure drop correlations developed from experiments and particle resolved direct numerical simulations (PR-DNS).

Earlier experiments were mostly focused on pressure drop measurement for given superficial velocity, Flow visualization technique such as particle image velocimetry (PIV) cannot be use due to lack of visibility in the bed. However Lebon et al. [6] measured velocities of flow inside the fixed bed using nuclear magnetic resonance (NMR) technique and reported distribution of normalized dominated velocity for Stokian flow which has single peak.

On the numerical side, the large number of curved and close proximity faces makes this simulation computationally expensive, and hence various techniques to simplify this simulation without significantly compromising the flow physics have been adopted. Gunjal et al. [7] used periodicity features of the flow and considered unit lattice structure to simulate single unit flow passage. They have considered various arrangements of spherical particles such as face-centered cubic (FCC), SC, 1D-Rhombohedral and 3D-Rhombohedral to realize effect of volume fraction on the flow resistance. The sensitivity of descritization showed the second-order accuracy is good enough to predict such flow physics. Rong et al. [8] used lattice botlzmann method (LBM) technique to simulate flow through randomly distributed sphere to study the effect of volume fraction for large range of Reynolds numbers. They have validated LBM results against Lebon et al experimental measurements. Wu et al. [9] used pore scale method to model the flow inside the fixed bed. In this study, the bed's complicated flow path is modeled using the network of nodes and pore-throat. The pore throat is a representation of the smooth converging-diverging flow passage formed by the arrangement of spherical particles. The pressure-velocity relation in the pore throat are modeled using the Hagen-Poiseuille equation, and iteratively velocity and pressure are calculated on each node on the network. The methodology is very promising to predict pressure drop and drag forces in the bed. However, the model performance for the non-spherical particles is not reported yet.

This paper explores the impact of sphericity on the flow resistance using PR-DNS simulation in Ansys Fluent 2019-R1 [10]. In PR-DNS, the unsteady Navier-Stokes equations are solved without any turbulence modelling, which demands highly refine grid refinement and small time scales to capture all the turbulent features. The sphericity is defined as the ratio of surface area of volume equivalent sphere to the particle surface area. The non-spherical particles such as cube, spheroid and tetrahedron are used to realize three different sphericities 0.92, 0.87, 0.67 in monosize BCC arrangement. The Reynold number from 10 to $10^4$ for air ($\rho = 1.225\ kg/m^3$, $\mu = 1.78x10^{-}5\ Pa\text{-}s$) is considered for close packing of particles with volume fractions (0.069-0.65), for which, the flow is mostly laminar. The air is assumed to be incompressible as the mach number encountered is quite lower than 0.3.

## PRESSURE DROP

The drop in pressure across the fixed bed system is a function of the shape of constitute particles, particle Reynolds number, and volume fraction. The volume fraction is defined as the solid volume ratio to the total volume of the bed. For stokes flow, the Blake-Kozeny-Carman equation [11] is widely used to predict pressure drop as given by Eqn. (1).

$$\frac{\Delta p}{L} = -\frac{\mu}{K}V, \text{ where } K = \frac{(1-\phi)^3 D_p}{150\phi^2} \tag{1}$$

where $\mu$ is the dynamic viscosity of fluid, L is the length of the bed, V is the velocity of fluid and K is the permeability of the bed. For high Reynold number regimes, Burk-Plummer equation is used, which takes dynamic pressure into account [12].

$$\frac{\Delta p}{L} = -\frac{\rho}{K}V^2, \text{ where } K = \frac{(1-\phi)^3 D_p}{1.75\phi} \tag{2}$$

Equation (1) mainly accounts for viscous effects and Eqn. (2) consider only inertia impact. Ergun [12] showed that pressure losses are concurrently governed by both kinetic and viscous energy losses and proposed Eqn. (3)

$$\frac{\Delta p}{L} = 150\frac{\phi^2}{(1-\phi)^3}\frac{\mu V}{D_p} + 1.75\frac{\phi}{(1-\phi)^3}\frac{\rho V^2}{D_p} \tag{3}$$

Lee et al. [13] tested this correlations and reported the errors due to turbulence at high Reynolds numbers. To account for such issue they have proposed new correlation shown in Eqn. (4) which is superior in high Reynolds number regime

$$\frac{\Delta p}{L} = \frac{12.5\phi^2}{(1-\phi)^3}(29.32Re^{-1} + 1.56Re^{-n} + 0.1)\frac{\rho V^2}{2}\frac{1}{D_p} \tag{4}$$

where, $n = 0.352 + 0.1(1-\phi) + 0.275(1-\phi)^2$.

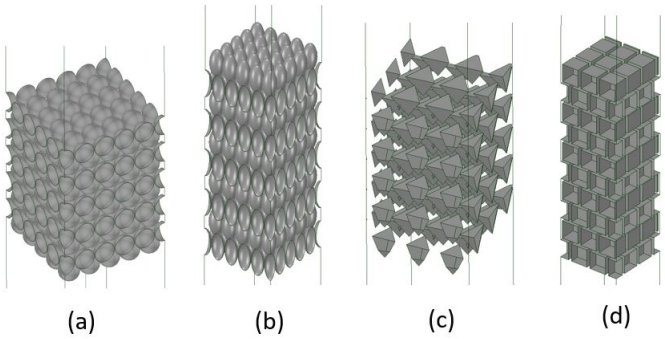


**Figure 1**. A ten layer bed of particles for (a) Sphere, (b) Spheroid, (c) Tetrahedron and (d) Cube with the lateral surface as periodic.

## CFD METHODOLOGY

The BCC arrangement of the spherical and non-spherical particles are created in the Ansys-SpaceClaim with around 200 particles in a cuboid flow passage with periodic lateral faces as shown in Fig. 1. The bottom face of the domain is set to velocity-inlet boundary condition and top face is set to pressure outlet. The particle diameter is 0.01 m with a bed height of 0.076 m in the domain of 0.05x0.05x0.8 m. Similarly, for non-spherical particles, the dominating sides or axial is kept at 0.01 m and Reynolds number is calculated using this length for all the particles. The domain is discretized with polyhedral cells using Ansys Fluent Mesher. Three different mesh settings were chosen, which gave cell count of 3, 6.4, and 20 million cells for spherical particles bed to understand the grid convergence as shown in Fig. 2. The drag coefficient ($C_d$) show in Eqn. 5 is measured for all the particles of the three meshes, and the measured values are averaged for the inner particles of the bed to avoid the effects of boundaries of the bed and periodicity.

$$C_d = \frac{2F_d}{\rho V^2 A_p} \tag{5}$$

Table 1 summarizes the important features of the mesh refinement. The grid refinement study showed the drag coefficient

**Table 1**. Summary of the grid independent study for Re=100 and $\phi$=0.65

| Mesh | Prism layers | Cells per gap | Cell Count (Millions) | $C_d$ |
|---|---|---|---|---|
| Refine-1 | 2 | 7 | 3 | 77.54 |
| Refine-2 | 4 | 10 | 6.4 | 77.50 |
| Refine-3 | 4 | 12 | 20 | 79.57 |

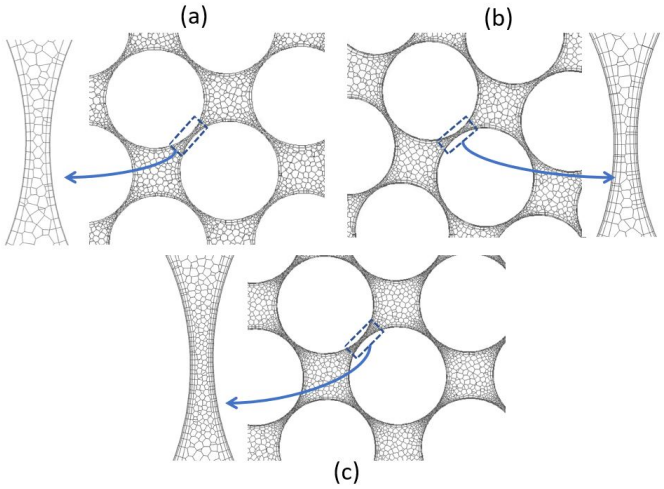


**Figure 2**. Polyhedral mesh of (a) 3 million, (b) 6.4 million and, (c) 20 million cells. The bottom image in each figure corresponds to the zoomed in version of the marked area and shows the packing and inter-particle distance.

calculated with all the three mesh settings is similar, but the normalized velocity distribution does not converge with time for 'Refine-1' mesh settings, i.e, the distribution of normalized velocity will keep fluctuating with time steps which is not expected for low Reynolds number flow. For the settings of 'Refine-2' and 'Refine-3', the normalized velocity distributions converges with time as shown in Fig. 3. The drag coefficient for individual particle is calculated which approaches a constant value within three layers of the bed and have minimum value for the last layer. Although all the three mesh settings predicted a similar drag coefficient, for this study, the settings of 'Refine-2' is adopted as a baseline for all the non-spherical cases, and additional curvature refinement is applied to improve mesh quality for the spheroid.

Transient pressure implicit with splitting of operators (PISO) solver with second-order accuracy for pressure, momentum, and temporal discretization is used with adaptive time stepping using CFL criteria of one with a minimum time step of 1e-8. The pressure drop across the bed for spherical particles is compared with Ergun (Eqn. (3)) and Lee et al. (Eqn. (4)) correlations, as shown in Fig. 4, one can observe the errors are significantly less in the low Reynolds number zone, where Ergun's correlations are superior. In the high Reynolds number area, Lee's correlations that take turbulent aspects of the flow into considerations are close to simulation predictions.

Regular particles spheroid, cube, and the tetrahedron are used to realize sphericity of 0.67 to 0.92 arranged in BCC arrangement to generate volume fractions in the range of 0.07-0.65. The study is limited to particles of high sphericity ($> 0.6$) to have a minimum dependency of the particle orientations on the drag coefficient [14]. In all the cases, the particles are not touching

each other to avoid unrealistic caping required to avoid acute angles. Figure 1 shows the bed of non-spherical particles used for this study, and the Table 2 summarizes the cases. The highest volume fractions for each particles is kept based on the minimum gap possible considering meshing complexities.

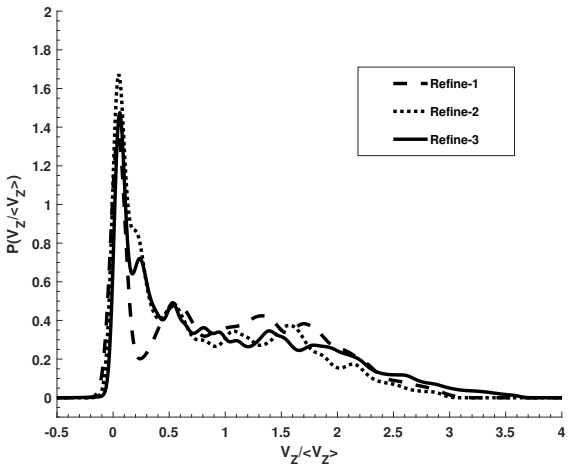


**Figure 3**. Probability density function of normalized z-component velocity.

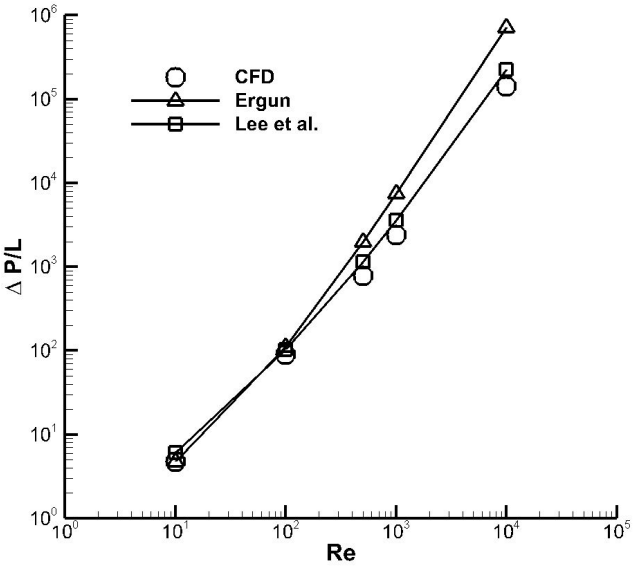


**Figure 4**. Comparison of pressure drop per unit length with correlations for bed of spherical particles with volume fraction $\phi = 0.65$. Symbol '◯', '□' and 'Δ' represents CFD, Eqn. (4) and Eqn. (3) respectively.

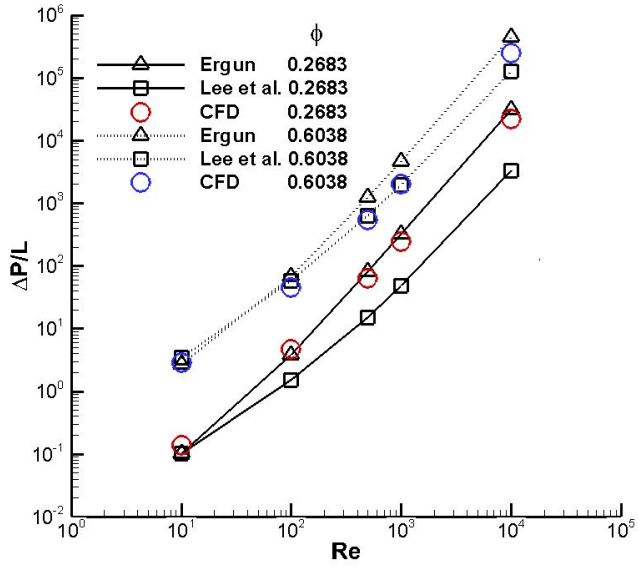


**Figure 5**. Effect of volume fraction($\phi$) on the pressure drop for cubic particles. Solid line and red color shows $\phi$=0.268 and dashed line and blue color shows $\phi$=0.6. Symbol '◯', '□' and 'Δ' represents CFD, Eqn. (4) and Eqn. (3) respectively.

## RESULTS AND DISCUSSION

The simulations of a bed of non-spherical particles show the significant dependency of its performance on the sphericity. The spheroid pressure drop characteristic shows large errors $(20-300\%)$ concerning Ergun's and Lee's correlations, increasing dramatically with Reynolds number. The cubic particle bed, which has non-curvilinear flow passages, gives a appreciable drag coefficient for a similar volume fraction compared to the sphere and spheroid having smooth curved surfaces. Interestingly, for low volume fractions, the pressure drop across this bed is very close to Ergun's prediction for all the Reynolds number as shown in Fig. 5. However, for large volume fractions, the pressure drop at a high Reynolds number remains uncertain but in the order of magnitude predicted by the correlations. In case of bed of tetrahedral particles also, the pressure drop pre-

**Table 2**. Summary of the fixed bed configuration studied

| Shape | $\psi$ | Volume fractions | Minimum-gap(x$10^{-4}m$) |
|---|---|---|---|
| Sphere | 1 | 0.65, 0.531, 0.4 and 0.23 | 0.4 |
| Spheroid | 0.92 | 0.592, 0.382 and 0.2693 | 0.4 |
| Cube | 0.805 | 0.604, 0.386 and 0.268 | 1.5 |
| Tetrahedron | 0.67 | 0.136, 0.177 and 0.07 | 1.65 |

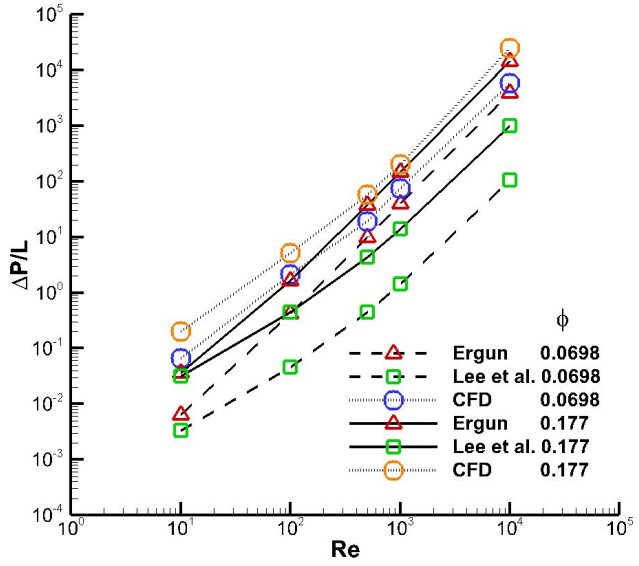


**Figure 6**. Comparison of pressure drop per unit length with correlations for bed of tetrahedral particles with volume fraction $\phi = 0.0698$ and $\phi = 0.177$. Symbol '◯', '□' and 'Δ' represents CFD, Eqn. (4) and Eqn. (3) respectively.

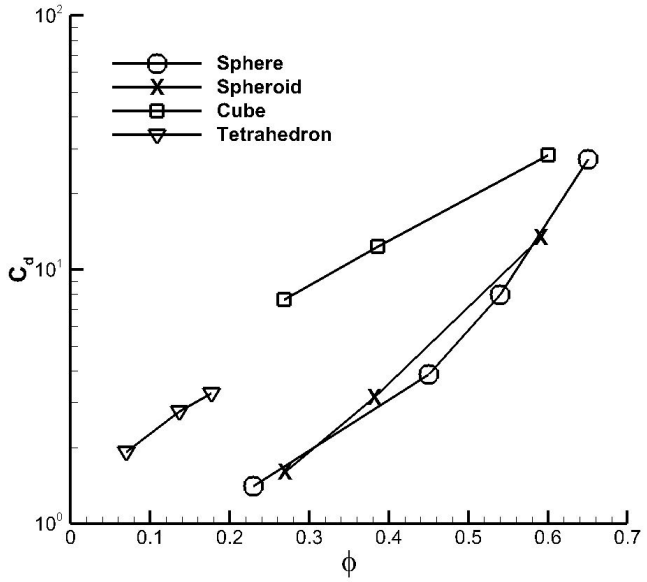


**Figure 7**. Effect of volume fraction ($\phi$) on the drag coefficient for Re=500. Symbol '◯','X','□' and '∇' represent the bed of Sphere, Spheroid, Cube and Tetrahedron respectively.

dictions are close to Ergun's correlation then Lee et al. as shown in Fig. 6. However, the pressure drop at low Reynolds number are under-predicted by both the correlations which might be due to the unavoidable large separation bubble behind the tetrahedron particles which kills the large part of fluid momentum.

Figure 7 shows the variation of drag coefficient with solid volume fraction for all the beds at Reynolds number 500. The low sphericity particles bed experiences a significantly large drag coefficient for volume fractions 0.1-0.5, and this difference reduces as volume fraction approaches to 0.6 or higher. It is noted that, the drag experienced by a bed of spheroid, which has high sphericity, is very close to that of bed of spherical particles. This dramatic variation in drag profile might be attributed to the sharp edges of the cube and tetrahedron and can be justified by analyzing Fig. 8 which shows the vector plot for tetrahedron particles. The high sphericity particles such as spheroid of Fig. 9 with low recirculation zone that allows flow to pass smoothly and hence experiences lowest drag. However, the low sphericity tetrahedron has a large recirculation bubble behind each particle that leads to a significant difference in pressure drop predicted by correlations. In addition to the sharp edges, the bed of tetrahedron particles also has larger fluid passages, allowing inertia force to dominate which generate a wider wake region giving rise to turbulence. On the other hand, the vector distribution around cubic particles shows the direct impingement of flow on the cube's flat front face which might be the reason for large drag forces. This phenomena is accurately captured in Fig. 10.

Figure 11 shows the drag coefficient variation for volume fraction with all the beds used in this study for two extreme Reynolds number 10 and $10^4$. At low Reynold number (Re=10) the effect of sphericity is not very strong and the drag coefficient can be strongly correlated using volume fraction itself. Also,

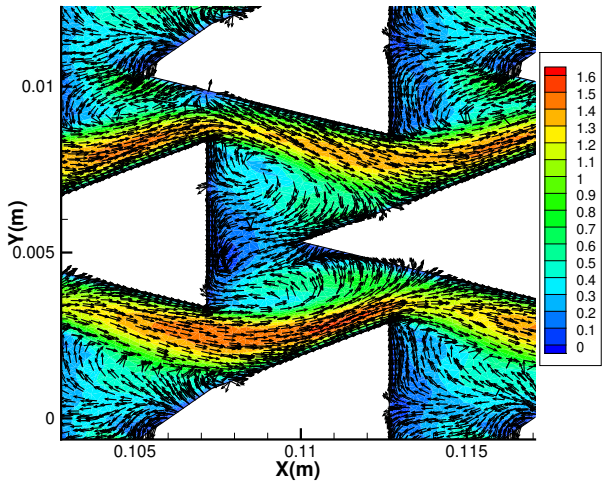


**Figure 8**. Cropped vector plot at Re=500, for the bed of tetrahedron. The vectors are superimposed on the contour of velocity magnitude (m/s)

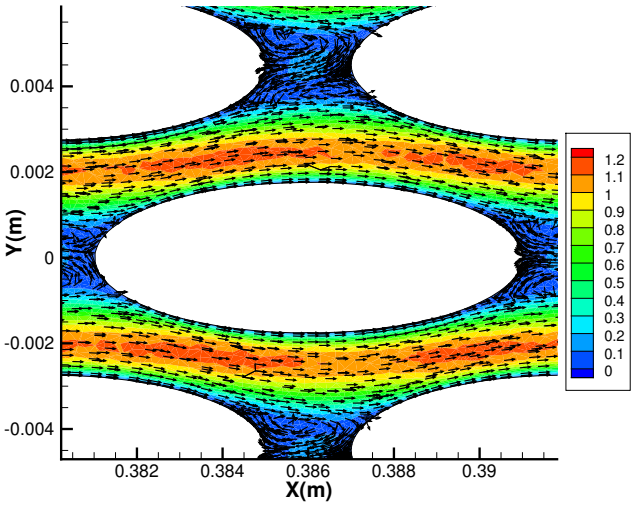


**Figure 9**. Cropped vector plot at Re=500, for the bed of spheroid. The vectors are superimposed on the contour of velocity magnitude (m/s)

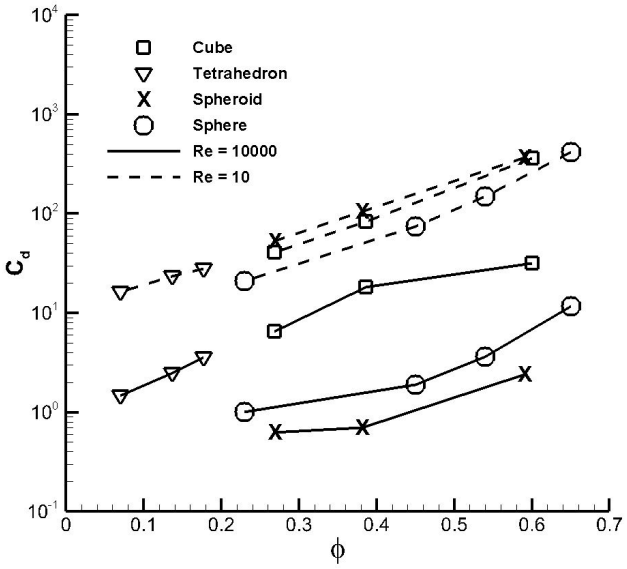


**Figure 11**. Effect of volume fraction ($\phi$) on the drag coefficient. Solid line shows Re=$10^5$ and dashed line shows Re=10. Symbol '◯','X','□' and '∇' represent the bed of Sphere, Spheroid, Cube and Tetrahedron respectively.

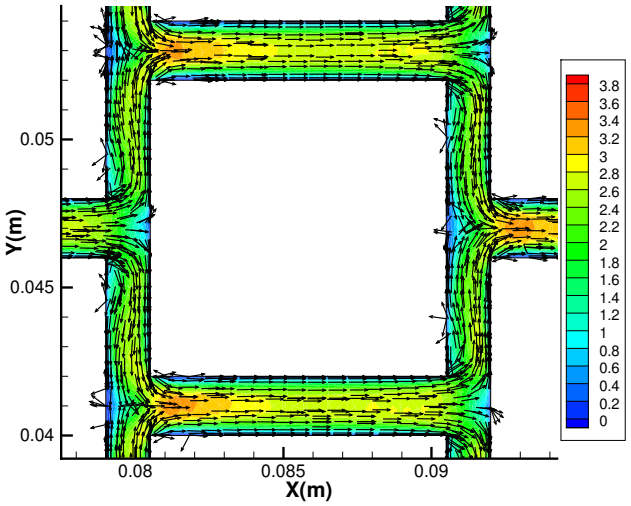


**Figure 10**. Cropped vector plot at Re=500, for the bed of cube. The vectors are superimposed on the contour of velocity magnitude (m/s)

the drag coefficient of spheroid is slightly higher than sphere as the flow is highly viscous dominated, so the force generated per unit projected area is higher for slightly slender body compared to bluff body. However for large Reynold's number the sphericity has strong impact on drag coefficient, as explain above the tetrahedron and cubic particle have very large drag coefficient where as spheroid experiences very low drag coefficient as pressure drag dominates in this regime of flow. However, for high Reynolds number the trend might change with the particles' orientation, especially for spheroids. Also, in this study the packing of particles are in BCC with virtual spaces between the particles. However, for real applications, the packing are generally random, and particles are touching each other. This random arrangement for low sphericity particle will affect drag forces if not the pressure drop.

## CONCLUSION

The PR-DNS for fixed-bed of non-spherical and spherical particles is conducted with variations in sphericity (0.65 to 1) and volume fractions (0.069-0.65) for Reynolds number 10 to $10^4$. The study utilizes the advantage of polyhedral mesh with low cell count compared to conventional tetrahedral mesh. The grid convergence study showed the refinement near the wall of the particles to capture boundary layer impacts the convergence of velocity profiles with time. Also, the methodology of periodicity is very effective in reducing computational power and time to predict pressure drop, which can be used to model the porous media approach for full bed numerical study.

The pressure drop for high Reynolds number is closely predicted by Ergun for spherical particles bed and for lower Reynolds number it is predicted by Lee et al. The study found the sphericity strongly affects the drag coefficient and bed pres-

sure drop. The pressure drop accross the bed of cubic particles with low volume fraction is closely matched with that of predicted by Ergun. Also, for the bed of tetrahedron, the pressure drop is closely predicted by Lee et al. for high Reynolds number but have large errors for low Reynolds number. The particles with edges have quite a different hydrodynamic effects compared to smooth surface particles and the differences are prominent in high Reynolds number regime. The drag coefficient of spheroid at high Reynolds number drops below sphere as its major axis is parallel to the flow which makes it more streamline than sphere. For future studies, the methodology will be extended for higher Reynolds number with adaptive grid refinement and effect of orientation of the particles on the drag coefficient and pressure drop will be considered.

## ACKNOWLEDGMENT

The authors would like to acknowledge the financial support from U.S. Department of Energy under award number DE-FE0031904

## REFERENCES

[1] Götz, M., Lefebvre, J., Mörs, F., Koch, A. M., Graf, F., Bajohr, S., Reimert, R., and Kolb, T., 2016. "Renewable power-to-gas: A technological and economic review". *Renewable energy,* ***85***, pp. 1371–1390.

[2] Mohan, D., and Pittman Jr, C. U., 2007. "Arsenic removal from water/wastewater using adsorbents—a critical review". *Journal of hazardous materials,* ***142***(1-2), pp. 1–53.

[3] Ouvrard, S., Simonnot, M.-O., and Sardin, M., 2002. "Reactive behavior of natural manganese oxides toward the adsorption of phosphate and arsenate". *Industrial & engineering chemistry research,* ***41***(11), pp. 2785–2791.

[4] Vollmari, K., Oschmann, T., Wirtz, S., and Kruggel-Emden, H., 2015. "Pressure drop investigations in packings of arbitrary shaped particles". *Powder Technology,* ***271***, pp. 109–124.

[5] Pozzobon, V., Colin, J., and Perre, P., 2018. "Hydrodynamics of a packed bed of non-spherical polydisperse particles: A fully virtual approach validated by experiments". *Chemical Engineering Journal,* ***354***, pp. 126–136.

[6] Lebon, L., Oger, L., Leblond, J., Hulin, J., Martys, N., and Schwartz, L., 1996. "Pulsed gradient nmr measurements and numerical simulation of flow velocity distribution in sphere packings". *Physics of Fluids,* ***8***(2), pp. 293–301.

[7] Gunjal, P. R., Ranade, V. V., and Chaudhari, R. V., 2005. "Computational study of a single-phase flow in packed beds of spheres". *AIChE Journal,* ***51***(2), pp. 365–378.

[8] Rong, L. W., Dong, K. J., and Yu, A., 2013. "Lattice-boltzmann simulation of fluid flow through packed beds of uniform spheres: Effect of porosity". *Chemical Engineering Science,* ***99***, pp. 44–58.

[9] Wu, Y., Hou, Q., and Yu, A., 2019. "Pore-scale study of fluid flow and drag force in randomly packed beds of different porosities". *Industrial & Engineering Chemistry Research,* ***58***(12), pp. 5041–5053.

[10] *Ansys® Academic Research Fluent, Release 2019 R1*.

[11] Burström, P. E., Frishfelds, V., Ljung, A.-L., Lundström, T. S., and Marjavaara, B. D., 2018. "Modelling heat transfer during flow through a random packed bed of spheres". *Heat and Mass Transfer,* ***54***(4), pp. 1225–1245.

[12] Ergun, S., 1952. "Fluid flow through packed columns". *Chem. Eng. Prog.,* ***48***, pp. 89–94.

[13] Lee, J. S., and Ogawa, K., 1994. "Pressure drop though packed bed". *Journal of chemical engineering of Japan,* ***27***(5), pp. 691–693.

[14] Bagheri, G., and Bonadonna, C., 2016. "On the drag of freely falling non-spherical particles". *Powder Technology,* ***301***, pp. 526–544.